Met. Mater. Int., Vol. 21, No. 1 (2015), pp. 22~30
doi: 10.1007/s12540-015-1004-x

Fatigue Crack Propagation Behavior of Fe24Mn Steel Weld at 298 and 110 K

Daeho Jeong[1], Soongi Lee[2], Insik Seo[2], Jangyong Yoo[2], and Sangshik Kim[1,*]

[1]Department of Materials Science and Engineering, ReCAPT, Gyeongsang National University, Chinju 660-701, Korea
[2]Plate Research Group, Technical Research Laboratory, POSCO, Pohang 790-785, Korea

(received date: 21 March 2014 / accepted date: 24 April 2014)

The fatigue crack propagation (FCP) tests were conducted on Fe24Mn steel in the region of base metal (BM), weld metal (WM) and fusion line (FL) at 298 and 110 K. The FCP rates of Fe24Mn specimens in the region of BM, WM and FL were greatly decreased, while no notable difference in the fracture mode was observed, with decreasing temperature from 298 to 110 K. The FCP rates of Fe24Mn WM and FL specimens were slightly lower than those of BM specimen at both room and cryogenic temperatures. The SEM fractographic analyses suggested that each specimen showed the transgranular facets at both temperatures in low and intermediate ΔK regimes. However, the morphological details varied depending on the region of weld and testing temperature. Relatively large sized facets were observed for the WM specimen with the columnar grain boundary playing the same role as the grain boundary in the BM and the FL specimens in the near-threshold ΔK regime. The FCP behavior of Fe24Mn steel in the region of BM, WM and FL is discussed at 298 and 110 K based on the fractographic and micrographic observation.

Keywords: alloys, welding, fatigue, fatigue crack propagation, low temperature

1. INTRODUCTION

With the world-wide increase in energy consumption, there is a great demand for steels in line pipe and offshore applications in seawater environments [1-3]. The austenitic stainless steels are important engineering alloys broadly used for such applications since they have excellent resistance to corrosion as well as good toughness and fatigue resistance over a wide range of temperature [4-7]. However, the wider application of austenitic stainless steels is limited due to their relatively low yield strength and high price [8-13]. To overcome the limitation, new high-manganese (Mn) austenitic steels are being developed, offering high yield strength and low cost [14,15]. High-Mn steels with Mn content of over 22% are, for example, are known to have promising low temperature tensile properties and fracture toughness [4,5,16]. In the near future, they are expected to replace expensive nickel (Ni)-containing steels used in LNG tankage and offshore structures in arctic environment [14,15,17]. The structures made of high-Mn steels may experience a variety of cyclic loading spectrums. The total life of such cyclic loaded component containing a crack-like flaw depends on the propagation rate of flaw from its original size to a critical size for final fracture and the major part of life is expended in the crack extension in low propagation rate regime [5,16,18]. It is therefore of practical importance to understand the fatigue crack propagation (FCP) behavior of high-Mn steels, particularly in the regime of low stress intensity factor range (ΔK).

For offshore and line pipe applications, a welding process is inevitably involved. Therefore, the effect of welding on the fatigue crack propagation (FCP) behavior of metals in service environments need to be well established. In general, the resistance to FCP of weld metal (WM) and heat affected zone (HAZ) of various steels are better or equal to those of the base metal (BM) [19,20]. The reasons are many-fold, including welding residual stress, the changes in microstructure and mechanical properties, weld micro-imperfections and crack tip morphology [16,21-24]. It has been shown that the distribution of residual stress arising after welding is complex and the magnitude varies with different regions of the weld. For example, the longitudinal residual stress, which acts along the welding direction, is known to be a maximum value in the WM and changed from tensile to compressive stresses as it moved away from the fusion zone. The transverse residual stress, on the other hand, varies symmetrically from compressive at the edges to tensile at the center of the plate [25]. The presence of compressive residual stress ahead of the crack tip will cause crack closure, reducing the FCP rates [21]. Such a distribution of residual stress may vary with the specimen machining and the propagation of crack, relieving the residual stress at the tip of crack. It has been argued that the FCP

*Corresponding author: sang@gnu.ac.kr

rates through the region of BM and WM become essentially the same when the residual stresses are relieved [25,26]. Small, rounded micro-imperfections like porosity and slag inclusions that in the weld may result in crack tip blunting, reducing the effective value of stress intensity. However, the beneficial effects of micro-imperfections are likely only if their size and number are below some critical value [27]. The coarse grain structure in the region of WM and HAZ may lower the FCP rates. Because of the complexities caused by the residual stress and the variety of metallurgical factors, the studies on the FCP behavior of steel welds are limited, despite the practical importance.

The present knowledge is further limited on the FCP behavior of steel weld at low temperatures. In general, the FCP rates and the near-threshold ΔK (ΔK_{th}) value, below which fatigue crack does not grow, increase with decreasing temperature for BCC (body-centered cubic) and FCC (face-centered cubic) materials [28,29]. Several mechanisms have been proposed. For example, compressive residual stress in the crack wake has been proposed to be responsible for the enhanced FCP resistance of some austenitic stainless steels at cryogenic temperatures as a result of deformation-induced phase transformation [30]. Other mechanisms include a diminished environmental effect [31], a reduced oxide-induced crack closure contribution [31,32], a change in failure mechanism from ductile to brittle manner [33] and an increase in stress to activate dislocation source located near the crack tip [32] at cryogenic temperatures. Among the proposed mechanisms, the previous studies on the FCP behavior of high-Mn steel at 110 K suggested that the mechanism associated with a dislocation dynamics model is predominant for the enhanced resistance to FCP at low temperatures [33]. At the tip of crack, the thermally activated energy available to move the dislocation over the barriers decreases with decreasing temperature, thereby resulting in an increase in the resistance to FCP at cryogenic temperatures.

In this study, the FCP behavior of Fe24Mn steel in the region of BM, WM and FL was investigated at 298 and 110 K. The crack paths and fracture surfaces were documented by using a scanning electron microscope (SEM) to identify any morphological changes in fracture surface with decreasing temperature. The FCP behavior of Fe24Mn austenitic steels was discussed based on the microstructural and the fractographic observations.

2. EXPERIMENTAL PROCEDURES

The Butt-welded Fe24Mn plate with the thickness of 30 mm was supplied by POSCO (Pohang, Korea) for the present study. The tensile property of Fe24Mn steel is summarized in Table 1. For the micrographic observation, the specimens were polished and etched by using a 2% Nital solution for 20~50 sec. Figure 1 shows the macrograph of Fe24Mn (a) weld and the optical micrographs documented in the region of (b) BM, (c) WM showing dendrite structure and (d) WM showing columnar grain boundaries. An austenite single phase with equi-axed grains of the average size of 38 μm was observed in the region of BM. The WM shows the typical dendritic structure with an average secondary dendrite arm spacing (SDAS) of 9 μm (Fig. 1(c)). The EBSD (electron backscatter diffraction) analysis was conducted for the clear observation of columnar grains in the weld (Figure 2). This figure shows that the average size of columnar grain

Table 1. Tensile properties of Fe24Mn steel at 298 and 110 K

Specimen	Temp. (K)	YS (MPa)	UTS (MPa)	Tensile elongation (%)
Fe24Mn	298	499	982	72
	110	778	1404	56

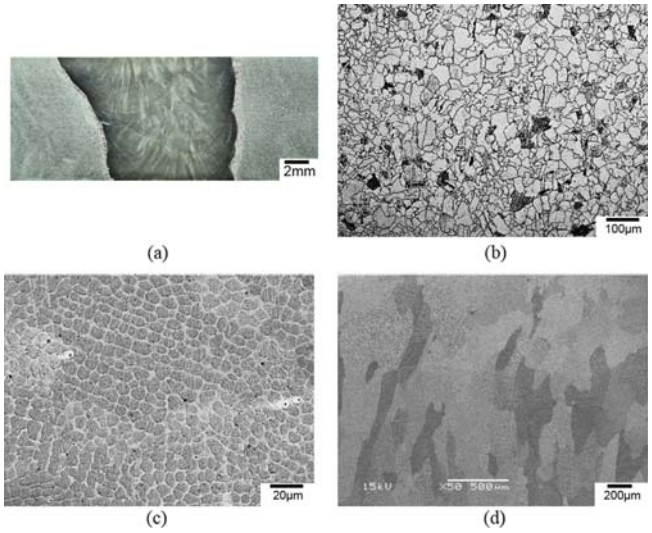

Fig. 1. The macrograph of Fe24Mn (a) weld and the optical micrographs documented in the region of (b) BM, (c) WM showing dendrite structure and (d) WM showing columnar grain boundaries.

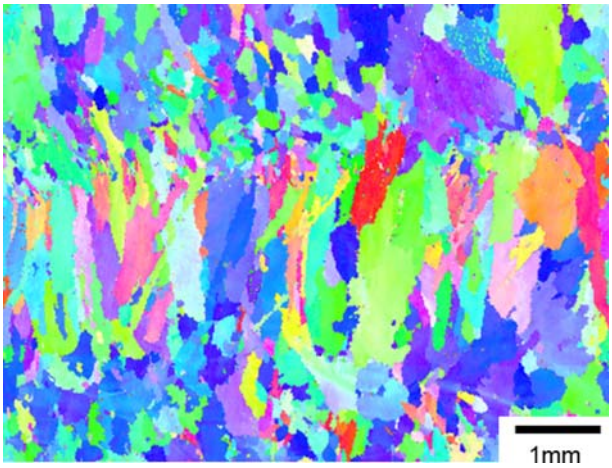

Fig. 2. The EBSD analysis result of Fe24Mn weld.

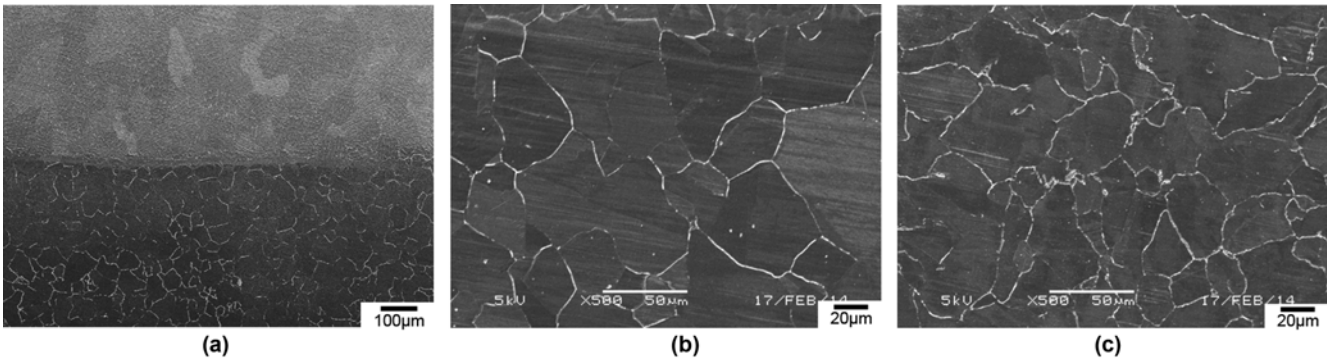

Fig. 3. The SEM micrographs of Fe24Mn weld in the region of (a) FL and (b) CGHAZ and (c) FGHAZ.

in the weld is 221 μm along the crack propagation direction. Figure 3 shows the SEM micrographs of Fe24Mn weld in the region of (a) FL and (b) coarse grain (CG) HAZ and (c) fine grain (FG) HAZ. The intergranular carbides (shown as while lines along the grain boundaries) were often observed in the HAZ, while more carbides were found in the FGHAZ than CGHAZ.

The compact tension (CT) specimens were prepared from the region of BM, WM and FL of the butt-welded Fe24Mn plate for the FCP tests. The FCP tests were carried out on the CT specimens at 298 and 110 K at an R ratio of 0.1 with a sinusoidal frequency of 10 Hz in accordance with ASTM E647 [34] using a servo-hydraulic testing machine (Instron Model 8516). Figure 4 shows the schematic illustrations of (a) CT specimen and (b) the location where the BM, the WM and the FL specimens were prepared. An environmental chamber, equipped with an electromechanically operated solenoid valve to control the gas flow of gasified nitrogen from cryogenic liquid nitrogen cylinder, was utilized to maintain the testing temperature of 110 K which is the temperature of LNG. The details of the low temperature fatigue testing system are described in the reference [5]. The fatigue crack length was automatically measured by using a DCPD (direct current potential drop) method. The SEM analyses were conducted on the FCP tested Fe24Mn specimens to observe the fracture mode. The broken half of the FCP tested specimen was mounted, polished and etched in Nital solution to observed the crack paths by using an optical microscope.

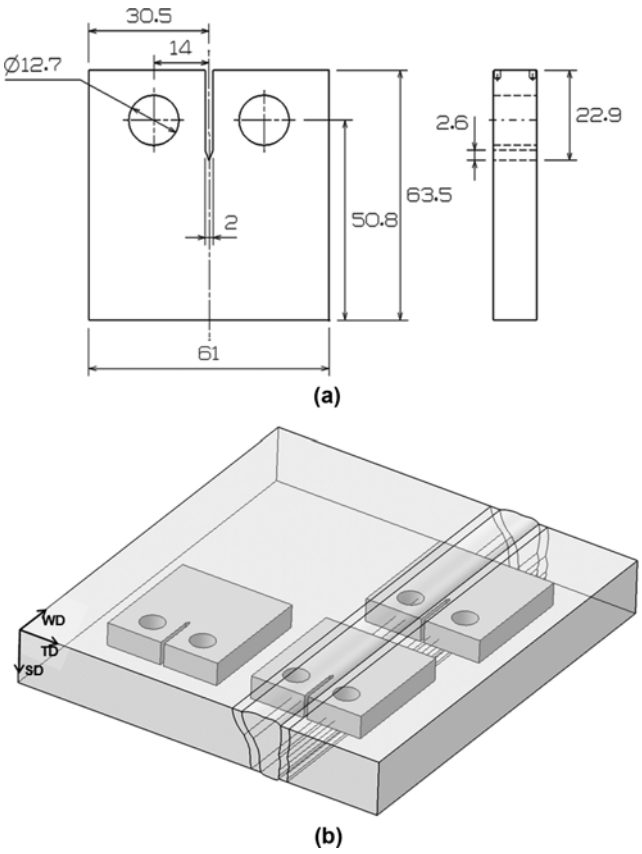

Fig. 4. The schematic illustrations of (a) CT specimen and (b) the locations where the specimens were prepared. All the units are mm.

3. RESULTS AND DISCUSSION

Figure 5 shows the *da*/*d*N (FCP rates)-ΔK curves of Fe24Mn specimen in the region of BM, WM and FL at 298 K. The FCP rates of Fe24Mn in the region of WM and FL were comparable with each other, while the BM specimen showed slightly higher FCP rates than the WM and the FL specimen, particularly in near-threshold ΔK regime. The ΔK_{th} value was, for example, 9.1, 11.4 and 12.1 MPa√m for the BM, the WM and the FL specimen, respectively, at 298 K and an R ratio of 0.1. It has been well established that the FCP rates in the region of WM and HAZ are generally lower, or comparable, to those of BM. The compressive residual stress acting at the tip of crack inducing crack closure is often considered to be responsible for the improvement in FCP resistance [22,25,35]. It is however extremely difficult to identify the distribution of residual stress at the tip of propagating crack through the weld, since the welding variables and the machining may all affect the profile of residual stress. In general, the transverse through-thickness residual stresses are tensile on the surface, while

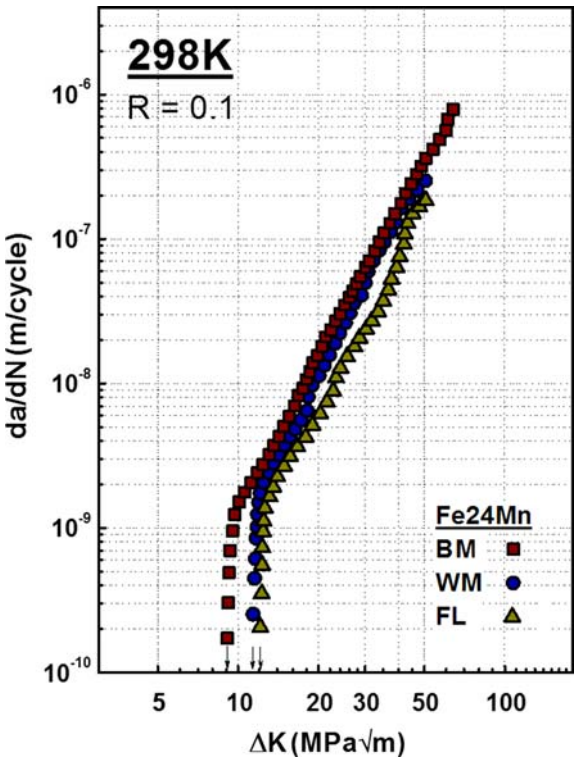

Fig. 5. The *da*/*d*N-ΔK curves of Fe24Mn specimens in the region of BM, WM and FL at 298 K.

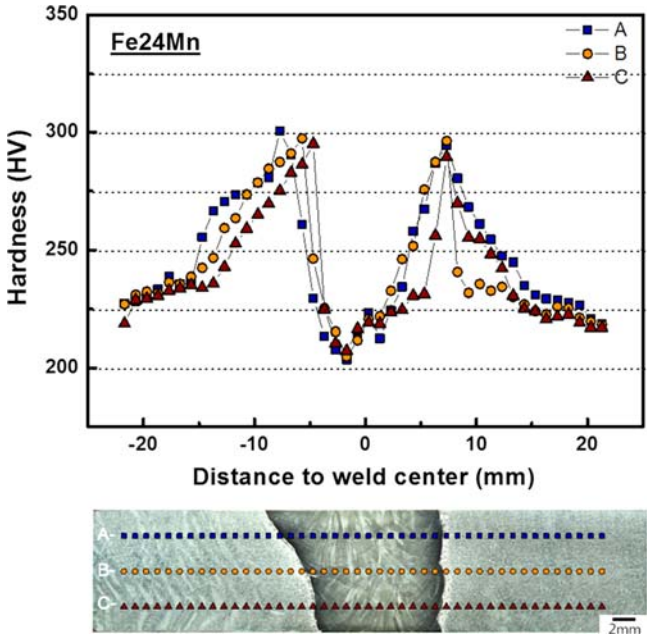

Fig. 6. The microhardness profiles across Fe24Mn weld.

they are compressive in the middle portion of butt-welded plate [36]. Since the CT specimen was prepared from the center portion of the butt-welded plate, the fatigue crack would be under the compressive residual stress. The longitudinal residual stresses along the weld direction, which is tensile in the center of the plate and becomes compressive as it moved away from the fusion zone, may also affect the FCP rates of the weld. The microhardness profiles across the weld in Fig. 6 indicated there was no notable difference in hardness between the surface and the middle portion of weld, suggesting that the magnitude of residual stress would not be significant in affecting the FCP behavior in the region of WM and FL in this study.

Other than the residual stress, the change in microstructure may affect the FCP behavior of Fe24Mn weld. To understand the influence of microstructure on the FCP rates of the weld, the SEM analysis was conducted on the FCP tested

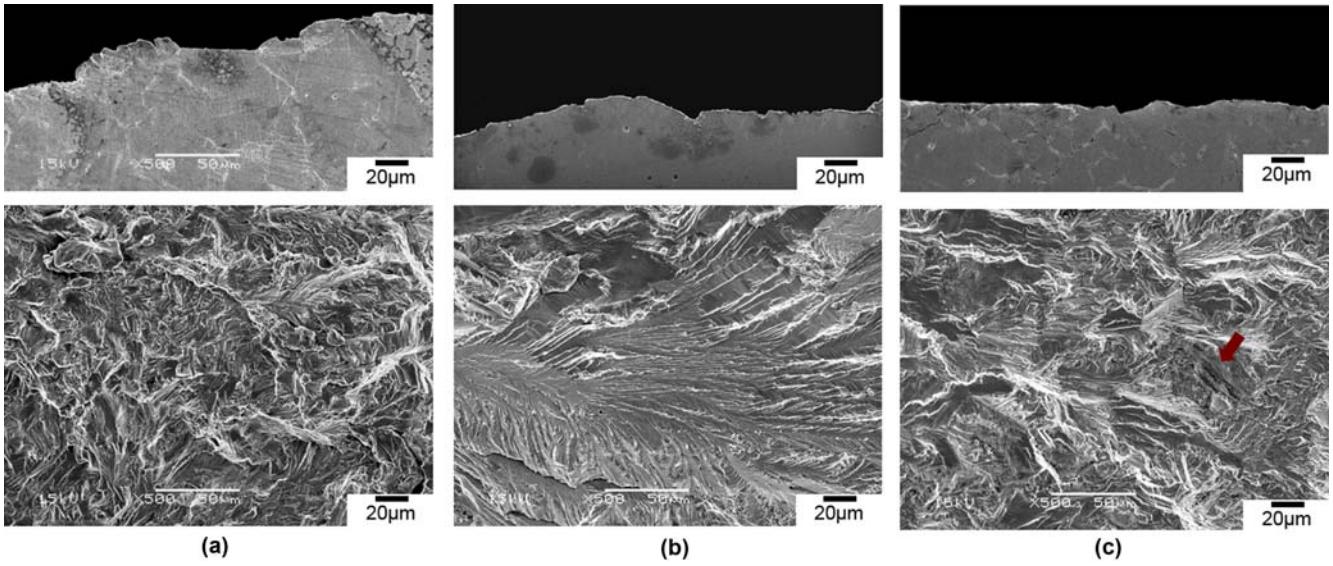

Fig. 7. The crack paths and SEM fractographs of FCP tested Fe24Mn specimens in the region of (a) BM, (b) WM and (c) FL, respectively, at 298 K in the near-threshold ΔK regime.

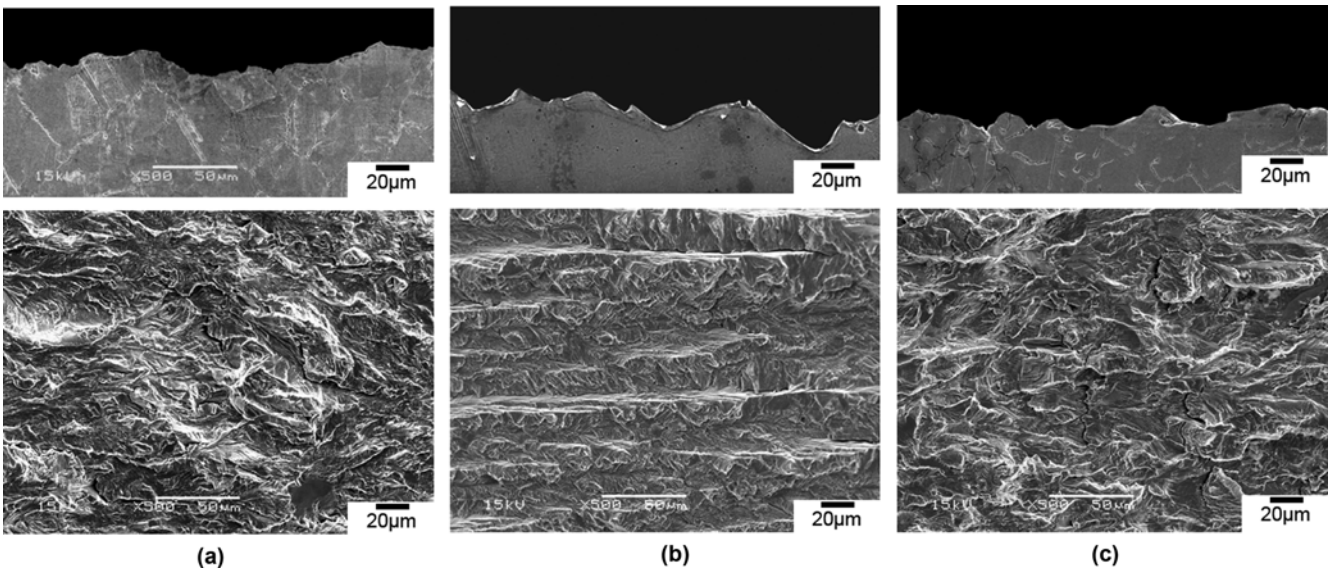

Fig. 8. The crack paths and SEM fractographs of FCP tested Fe24Mn specimens in the region of (a) BM, (b) WM and (c) FL, respectively, at 298 K at ΔK of 30 MPa√m.

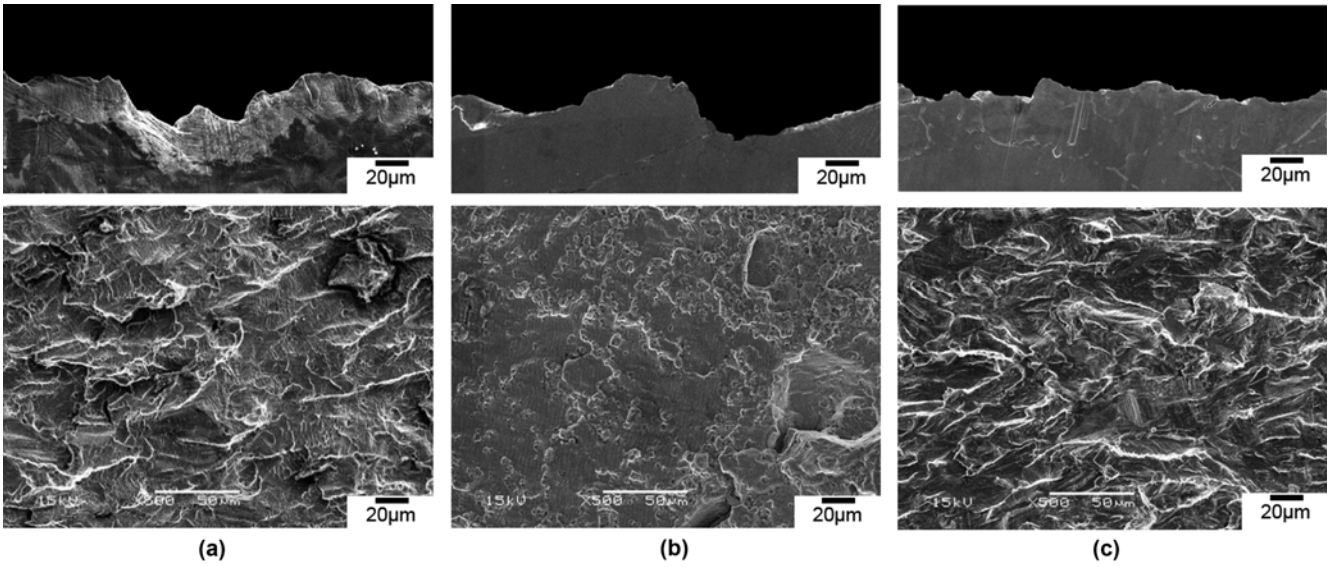

Fig. 9. The crack paths and SEM fractographs of FCP tested Fe24Mn specimens in the region of (a) BM, (b) WM and (c) FL, respectively, at 298 K at ΔK of 50 MPa√m.

specimens in different ΔK regimes. Figures 7, 8 and 9 show the crack paths and the SEM fractographs of the FCP tested Fe24Mn specimens at room temperature in the region of (a) BM, (b) WM and (c) FL, respectively, in the near-threshold ΔK regime (Fig. 7) and at the ΔK of 30 MPa√m (Figure 8) and 50 MPa√m (Fig. 9). The crack propagation direction was from left to right. In the near-threshold ΔK regime, the transgranular cleavage facets were shown on the fracture surface for all the specimens. However, the morphological features of such facets were substantially different from one another. For the BM specimens, the average size of facet was approximately 50 μm that matched to the size of grain. The crack path in Fig. 7(c) showed that for the FL specimens, the crack propagated through the CGHAZ which was about 840 μm away from the fusion line. The grain size of this region of CGHAZ was approximately 77 μm, and the average facet size for the FL specimen was 65 μm which was larger than that for the BM specimen. As shown in Fig. 3, the intergranular carbides were often observed in the region of CGHAZ. The SEM fractographic and crack path analyses, however, did not show any notable influence of carbide on the FCP behavior, such as crack blocking, carbide-debonding or carbide-breakage. Only a very limited number of carbide debonding was observed on the fracture surface, as indicated by the arrow in Fig. 7(c),

where the carbides were located favorably to the direction of crack propagation. Marginal influence of carbide in the region of CGHAZ near the FL was probably due to the transgranular crystallographic nature of crack propagation. In other words, the effect of intergranular carbides on the transgranular FCP behavior of Fe24Mn weld was not significant. Interestingly, the size of facet for the WM specimen was 193 μm which was much greater than that for the BM and the FL specimens in the near-threshold ΔK regime. The micrographs in Figs. 1 and 2 indicate that the facet size for the WM specimens roughly matches to that of columnar grain size, suggesting that the individual dendrite did not affect the FCP behavior of Fe24Mn weld in the near-threshold ΔK regime. With increasing ΔK to 30 MPa√m, the fracture mode of transgranular cleavage facet was still predominant for the BM and the FL specimens, as shown in Figure 8. As compared to those in the near-threshold ΔK regime, the fracture surface tended to be relatively flat with increasing ΔK and show the tendency for mode I FCP perpendicular to the loading direction. Unlike the other two specimens, the fracture mode of the WM specimen at ΔK of 30 MPa√m was completely different from that in the near-threshold ΔK regime. The steps parallel to the crack propagation direction were observed on the fracture surface, and each step appeared to be divided by fine facets. The spacing between these steps roughly matched to the size of dendrite arm spacing. It was therefore suggested that the dendritic structure affected the FCP behavior of Fe24Mn weld in the Paris' regime, while the columnar grain boundaries played the same role in the near-threshold ΔK regime. With further increase in ΔK to 50 MPa√m, all the specimens showed mode I crack propagation with striations (Fig. 9). The influence of microstructure on the FCP behavior is then greatly reduced in this upper stage II region, and the crack propagates perpendicular to the loading direction forming the striations as a result of massive slip deformation at the tip of crack and slip irreversibility.

Figure 10 schematically illustrates the change in FCP mechanism for the Fe24Mn specimens in the region of (a) BM and FL, and (b) WM at room temperature. For the BM and FL specimens, the fatigue crack propagates along certain cleavage planes within the grain in the near-threshold ΔK regime. The crystallographic plane changes at the grain boundaries forming the facets with the size similar to that of grain. As the crystallographic slip deformation is blocked by grain boundary, the extent of strain localization depends on the grain size. Therefore, the smaller grain size tends to reduce the slip length and the slip reversibility, reducing the resistance to FCP in the near-threshold ΔK regime [37-39]. With increasing ΔK, the ratio of reversed plastic zone size to grain size becomes the rate-controlling factor when grain boundary is the major barrier to slip [40,41]. When the grain size is smaller than the reversed plastic zone, high local stress concentrations at the head of the pileup will induce slip on secondary slip systems in the same grain as well as slip in

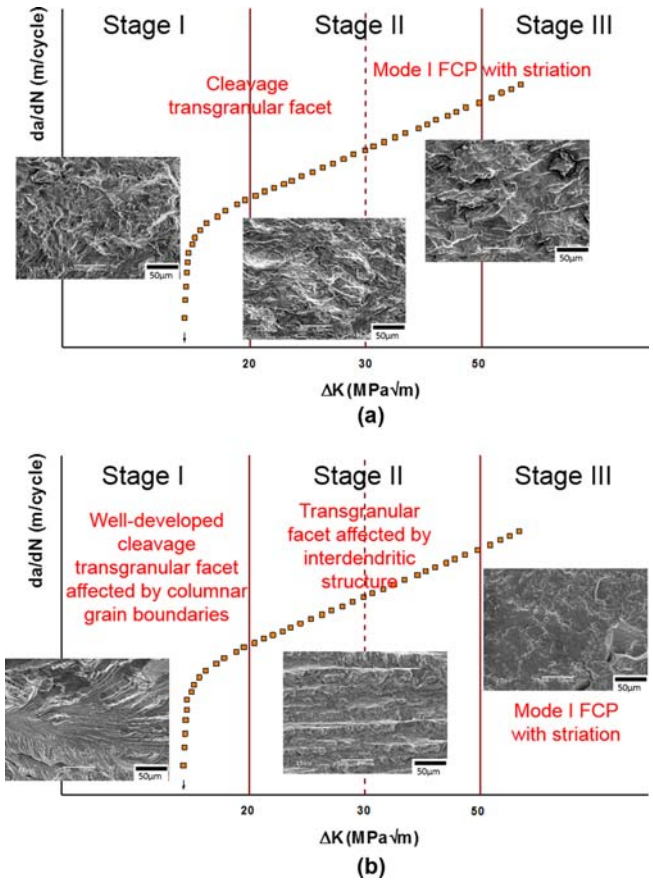

Fig. 10. The schematic illustration of FCP mechanisms for the Fe24Mn specimens in the region of (a) BM and FL, and (b) WM at 298 K.

neighboring grains and multiple slip is activated even in planar slip materials [21]. With such an FCP mechanism changes, the fracture mode also changes from transgranular cleavage facets along certain crystallographic plane to mode I FCP perpendicular to the loading direction with massive slip deformation at the crack tip and the striations left behind the crack. For the WM specimen, the columnar grain boundary plays the same role as grain boundary in the BM and the FL specimens in the near-threshold ΔK regime, forming large facets matching to the size of columnar grain. With increasing ΔK, the crack in the region of WM follows the interdendritic region forming steps on the fracture surface.

Figure 11 shows the *da*/*d*N-ΔK curves for the Fe24Mn specimens in the region of BM, WM and FL at 110 K. The comparison between Figures 5 and 11 indicated that the FCP resistance of Fe24Mn BM specimen was greatly improved with decreasing temperature from 298 to 110 K, which was previously reported in the reference [5]. This study showed that the same trend of reducing FCP rates for the Fe24Mn specimens in the region of WM and FL with decreasing temperature from 298 to 110 K. Other than the reduction in the FCP rates, the overall trend in the FCP behavior of Fe24Mn

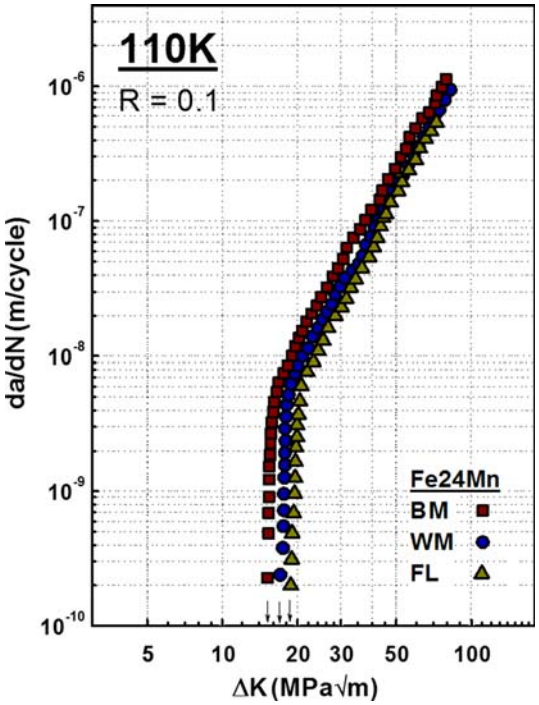

Fig. 11. The da/dN-ΔK curves of Fe24Mn specimens in the region of BM, WM and FL at 110 K.

specimen at 110 K was similar to that at room temperature the FCP rates of the WM and the FL specimens were comparable with each other, while they showed slightly better FCP resistance than the BM specimen in near-threshold ΔK regime. The ΔK_{th} value, for example, was 15.2, 17.1 and 18.5 MPa√m for the Fe24Mn specimens in the region of BM, WM and FL, respectively, at 110 K. Previously, several possible mechanisms for the improvement in FCP behavior of Fe24Mn BM specimen with decreasing temperature were assessed by the authors [5]. The mechanisms include the diminished environmental effect [15], the reduced oxide-induced crack closure contribution [13,42], the change in failure mechanism from ductile to brittle manner [40] and the increase in stress to activate dislocation source located near the crack tip [32] at cryogenic temperatures. Among them, the mechanism associated with a thermal stress for activating dislocation source was proposed for the low temperature improvement in FCP resistance of high-Mn austenitic steels [5]. At the tip of crack, the thermally activated energy available to move the dislocation over the barriers decreases with decreasing temperature, thereby reducing the FCP rates of Fe24Mn BM specimen at 110 K.

Figures 12 and 13 show the crack paths and the SEM fractographs of the FCP tested Fe24Mn specimen in the region of (a) BM, (b) WM and (c) FL, respectively, at 110 K in the near-threshold ΔK regime (Fig. 12) and at ΔK of 30 MPa√m (Fig. 13). The crack propagation direction was from left to right. No notable change in the fracture mode was observed for the BM and the FL specimen with decreasing temperature from 298 to 110 K. The transgranular cleavage facets were also observed at 110 K for the BM and the FL specimens in the near-threshold ΔK and lower stage II regimes, similar to those observed at room temperature. For the WM specimens, on the other hand, notable difference in fracture mode was observed with decreasing temperature from 298 to 110 K in the near-threshold ΔK regime. The transgranular facets across the columnar grains were still observed for the WM specimen at 110 K. Unlike those at 298 K, the transgranular facet in the region of WM at 110 K was flat and featureless with shallow river marks along the direction of crack propagation. At ΔK of 30 MPa√m, the fracture appearance of WM specimen at 110 K also showed a notable difference

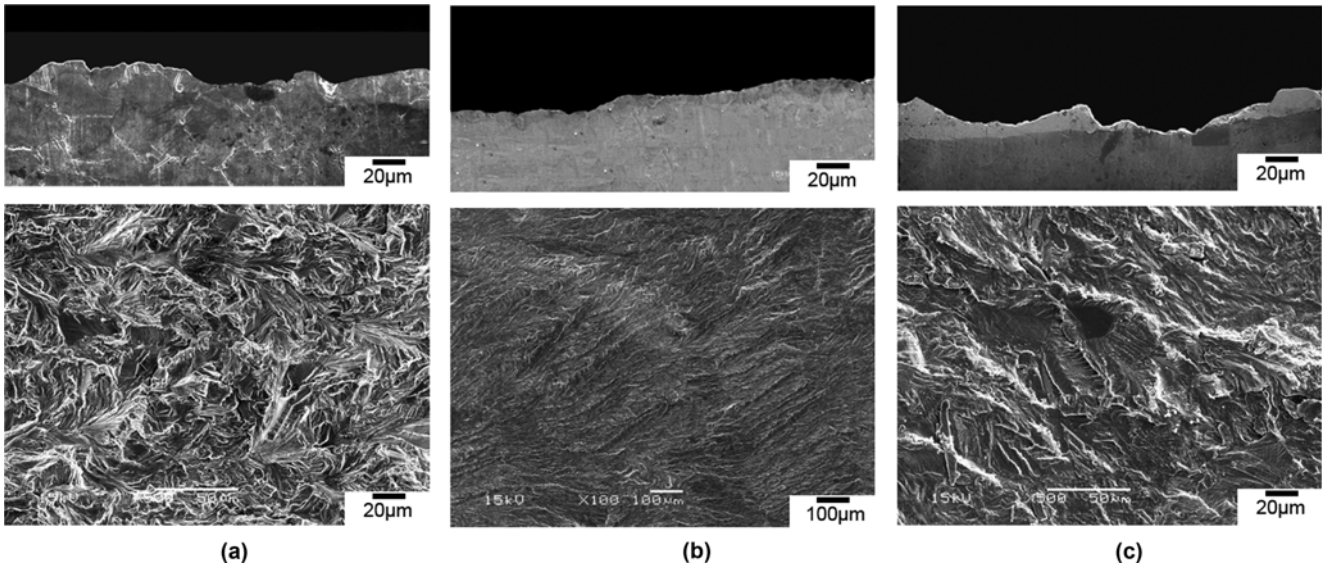

Fig. 12. The crack paths and SEM fractographs of FCP tested Fe24Mn specimens in the region of (a) BM, (b) WM and (c) FL, respectively, at 110 K in the near-threshold ΔK regime.

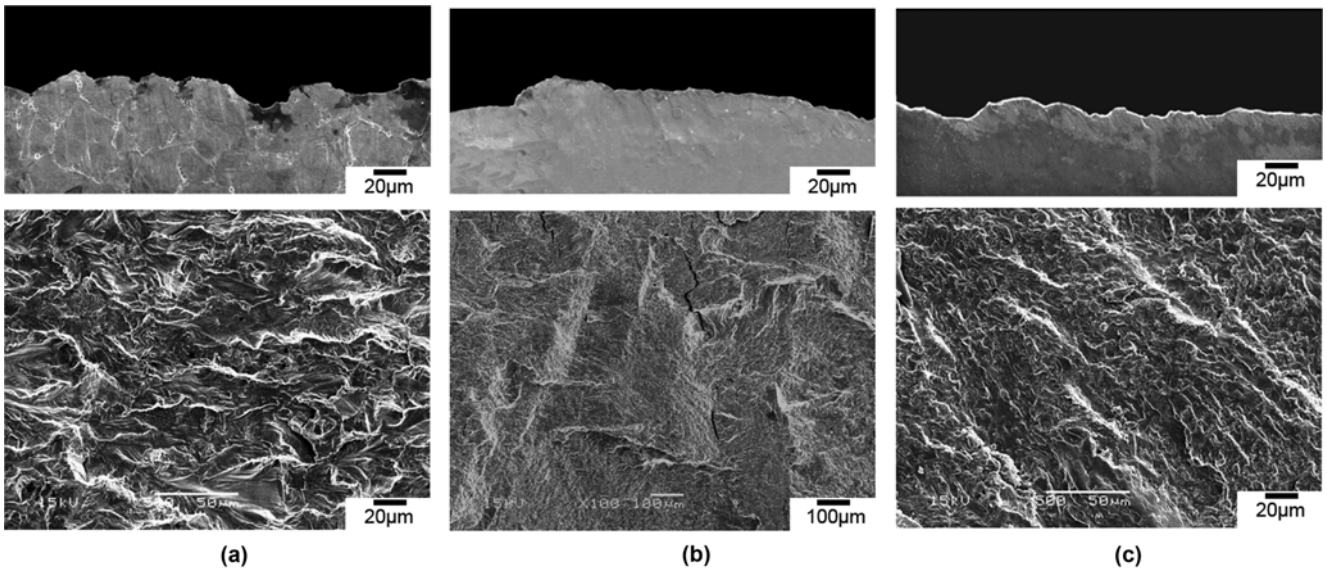

Fig. 13. The crack paths and SEM fractographs of FCP tested Fe24Mn specimens in the region of (a) BM, (b) WM and (c) FL, respectively, at 110 K at ΔK of 30 MPa√m.

as compared to that at room temperature. The fracture surface appeared to be flat and featureless, unlike the step-like fracture mode at room temperature. It was also noted that the effect of barriers blocking crack propagation, including the columnar grain boundaries in the near-threshold ΔK regime and the interdendritic boundaries in the intermediate ΔK regime, was not as significant as that at room temperature. It was therefore hypothesized that the crystallographic plane for transgranular crack propagation of Fe24Mn weld would change from low index plane to high index plane with decreasing temperature. Indeed, Mohseni et al. have identified by EBSD study that the crystallographic indices of the cleavage crack planes for X80 steel was {100}, {110}, {211} and {310} [42]. They further proposed that the tendency for the {110} facet increased, while that for {100} facet decreased, with decreasing temperature. The slip deformation at the tip of crack is determined in a complex manner by the constraint for maintaining the continuity and the available habit index planes. The possibility of cleavage facet planes confined only on certain crystallographic planes is higher for the case of low index planes than that of high index planes. The fracture appearance is then flatter and smoother at low temperatures with high index planes than at room temperature with low index planes. The present fractographic analysis of Fe24Mn suggested that the proposed mechanism for the improved FCP resistance of high-Mn austenitic steels at cryogenic temperatures would be also applicable for the WM and FL specimens. As shown in Figures 12 and 13, the WM and FL specimens show the transgranular cleavage faceting in the near-threshold ΔK and the lower stage II regimes. The transgranular faceting along certain crystallographic planes is basically determined by the critical stress activating dislocation movement at the tip of crack. The mechanism based on dislocation dynamics model for the Fe24Mn BM is therefore believed to be applicable for the WM and FL specimens.

4. CONCLUSIONS

In the present study, the FCP tests were conducted on the Fe24Mn specimens in the region of BM, WM and FL at 298 and 110 K, and the following conclusions were drawn.

(1) At room temperature, the FCP rates of Fe24Mn in the region of WM and FL were comparable with each other, while the BM specimen showed slightly higher FCP rates than the WM and FL specimens, particularly in near-threshold ΔK regime.

(2) The fatigue crack for the BM, WM and FL specimens propagated crystallographically within the grain in the near-threshold ΔK regime. The crystallographic plane changed at the grain boundaries forming the facets with the size similar to that of grain. For the WM specimen, the columnar grain boundary played the same role as grain boundary in the BM and the FL specimens in the near-threshold ΔK regime, forming relatively large facets matching to the size of columnar grain. With increasing ΔK, the crack in the region of WM followed the interdendritic region forming steps on the fracture surface.

(3) The FCP behavior of Fe24Mn specimens in the region of BM, WM and FL was greatly improved with decreasing temperature from 298 to 110 K. Other than the increase in FCP resistance, the overall trend in the FCP behavior of Fe24Mn at 110 K was similar to that at room temperature.

(4) The transgranular cleavage facets were also observed

at 110 K for the BM and FL specimens in the near-threshold ΔK and lower stage II regimes, similar to those observed at room temperature. The transgranular facet in the region of WM at 110 K tended to be flat and featureless along the direction of crack propagation in the near-threshold and intermediate ΔK regimes.

ACKNOWLEDGMENTS

This work was supported by the National Research Foundation of Korea (NRF) grant funded by the Korea government (MSIP) (2011-0030058). This research was also supported by the Development of Drill Riser System Project (14-9807) of the KIGAM funded by the Ministry of Knowledge Economy of Korea.

REFERENCES

1. J. Billingham, J. V. Sharp, J. Spurrier, and P. J. Kilgallon, *Research Report 105*, pp.1-111, Health and Safety Executive (HAE) Books, Cranfield (2003).
2. NORSOK Standard M-001, Rev. 3, pp.7-23, Norway (2002).
3. J. K. Kwon, D. H. Ahn, D. H. Jeong, Y. J. Kim, N. S. Woo, and S. S. Kim, *Korean J. Met. Mater.* **52**, 757 (2014).
4. D. T. Read and R. P. Reed, *Cryogenics*, **21**, 415 (1981).
5. D. H. Jeong, S. G. Lee, W. K. Jang, J. K. Choi, Y. J. Kim, and S. S. Kim, *Metall. Trans. A*. **44A**, 4601 (2013).
6. K. S. Bang, S. H. Pak, and S. K. Ahn, *Met. Mater. Int.* **19**, 1267 (2013).
7. Z. Mei and J. W. Morris, Jr., *Metall. Trans. A*. **21A**, 3137 (1990).
8. R. L. Tobler and R. P. Reed, *J. Test. Eval*. **12**, 364 (1984).
9. J. K. Kwon, H. Y. Lee, Y. J. Kim, and S. S. Kim, *Korean J. Met. Mater.* **49**, 774 (2011).
10. J. W. Morris, Jr., J. W. Chan, and Z. Mei, *Fourteenth International Cryogenic Engineering Conference and International Cryogenic Materials Conference*, p.1, Keiv, Ukraine (1992).
11. Y. S. Yoon, H. Y. Ha, T. H. Lee, and S. S. Kim, *Corros. Sci.* **80**, 28 (2014).
12. N. B. Fredj and H. Sidhom, *Cryogenics*, **46**, 439 (2006).
13. D. Y. Ryoo, S. C. Lee, Y. D. Lee, and J. Y. Kang, *Met. Mater. Int*. **7**, 1381 (2001).
14. R. Ogawa and J. W. Morris, Jr., *Fatigue at Low Temperatures*, ASTM STP 857, p.47, R.I. Stephens, ed., American Society for Testing and Materials, Philadelphia (1985).
15. Q. Dai, R. Yang, and K. Chen, *Materials Characterization*, **42**, 21 (1999).
16. D. H. Jung, J. K. Kwon, N. S. Woo, Y. J. Kim, M. Goto, and S. S. Kim, *Metall. Trans. A*. **45A**, 654 (2014).
17. T. Yokobori, I. Maekawa, Y. Tanabe, Z. Jin, and S. I. Nishida, *Fatigue at Low Temperatures*, ASTM STP 857, p.121, R. I. Stephens, ed., American Society for Testing and Materials, Philadelphia (1985).
18. S. S. Kim, J. K. Kwon, Y. J. Kim, W. K. Jang, S. G. Lee, and J. K. Choi, *Met. Mater. Int*. **19**, 1 (2013).
19. M. A. N. Beltrao, E. M. Castrodeza, and F. L. Bastian, *Fatigue Fract. Engng. Mater. Struct*. **34**, 321 (2010).
20. L. W. Tsay, T. S. Chern, C. Y. Gau, and J. R. Yang, *Int. J. Fatigue*. **21**, 857 (1999).
21. E. A. Starke and J. C. Williams, in *Fracture Mechanics, Perspectives and Directions*, ASTM STP 1020, p.184, R. P. Wei and R. P. Gangloff, eds., American Society for Testing and Materials, Philadelphia (1989).
22. G. Deqing, *Int. J. Fatigue*. **18**, 221 (1996).
23. S. Suresh, *Metall. Trans. A*. **14A**, 2375 (1983).
24. S. Suresh, *Metall. Trans. A*. **16A**, 249 (1985).
25. T. Ninh Nguyen and M. A. Wahab, *J. Mater. Process. Technol.* **77**, 201 (1998).
26. R. Galatolo and A. Lanciotti, *Int. J. Fatigue*. **19-1**, 43 (1997).
27. C. D. Donne, G Biallas, T. Ghidini, and G. Raimbeaux, *Proceedings of the second international symposium on friction stir welding*, p.1, Gothenburg, Sweden (2000).
28. L. Baotong and Z. Xiulin, *Mater. Sci. Eng*. **A148**, 179 (1991).
29. K. A. Esaklul, W. Yu, and W. W. Gerberich, *Fatigue at Low Temperatures*, ASTM STP 857, p.63, R. I. Stephens, ed., American Society for Testing and Materials, Philadelphia (1985).
30. L. Lawson, E. Y. Chen, and M. Meshii, *Int. J. Fatigue*. **21**, S15 (1999).
31. P. K. Liaw and W. A. Logsdon, *Eng. Fract. Mech*. **22**, 585 (1985).
32. W. Yu, K. Esaklul, and W. W. Gerberich, *Metall. Trans. A*. **15A**, 889 (1984).
33. R. L. Tobler and Y. W. Cheng, *Fatigue at Low Temperatures*, ASTM STP **857**, 3 (1985).
34. ASTM Standard E647, *Standard test method for measurement of fatigue crack growth rates*, Annual book of ASTM standards, 03.01 (2002).
35. H. T. Kang, Y. L. Lee, and X. J. Sun, *Mater. Sci. Eng*. **A497**, 37 (2008).
36. FITNET final technical report MK7, Annex C, pp.6-9 (2006).
37. E. Hornbogen and K. H. Zum Gahr, *Acta Metallurgica*, **24**, 581 (1976).
38. S. B. Chakrabortty, *Fatigue in Engineering Materials and Structures*. **2**, 331 (1979).
39. S. Majumdar and J. D. Morrow, *in Fracture Toughness and Slow-Stable Cracking*, (Eighth Conference), p.159, ASTM STP 559, American Society for Testing and Materials, Philadelphia (1974).
40. J. L. Robinson and C. J. Beevers, *Metall. Science. J.* **7**, 153 (1973).
41. J. Lindigkeit, G. Terlinde, A. Gysler, and G. Lutjering, *Acta Metallurgica*, **27**, 1717 (1979).
42. P. Mohseni, J. K. Solberg, M. Karlsen, O. M. Akselsen, and E. Østby, *Deformation of Crystallographic Facet Orientations on Fracture Surfaces of an Arctic Steel by Using EBSD* Proceedings of the twenty-second international offshore and polar engineering conference, Rhode, Greece, June, 305 (2012).